Article

An Efficient Hydrogen-Generation CuO/Co3O4 Heterojunction Nanofibers for Sensitive Detection of Cancer Cells by Portable Pressure Meter

Erli Ding, Jun Hai, Tianrong Li, Jie Wu, Fengjuan Chen, Yin Wen, Baodui Wang, and Xiaoquan Lu

Anal. Chem., **Just Accepted Manuscript** • DOI: 10.1021/acs.analchem.7b01951 • Publication Date (Web): 06 Jul 2017

An Efficient Hydrogen-Generation CuO/Co_3O_4 Heterojunction Nanofibers for Sensitive Detection of Cancer Cells by Portable Pressure Meter

Erli Ding[†], Jun Hai[†], Tianrong Li[†], Jie Wu[†], Fengjuan Chen[†], Yin Wen[§], Baodui Wang[†,*], and Xiaoquan Lu[‡,*]

[†]Key Laboratory of Nonferrous Metal Chemistry and Resources Utilization of Gansu Province and State Key Laboratory of Applied Organic Chemistry Lanzhou University Gansu, Lanzhou, 730000 (P.R. China) Lanzhou University, Lanzhou 730000, P. R. China.

[‡]Department of Chemistry, Tianjin University, Tianjin 300072, P. R. China.

[§]Department of Pharmacy, Lanzhou University Second Hospital, Lanzhou, Gansu, Lanzhou 730000, P. R. China.

ABSTRACT

Portable, low-cost, and quantitative detection of cancer cells at home and in the field has the potential to revolutionize medical diagnostics. We first report the design and synthesis of highly efficient folic acid-conjugated hydrogen-generation tube-in-tube CuO/Co_3O_4 heterojunction nanofibers for highly sensitive and rapidly recognition of cancer cells through pressure signal under visible light irradiation. The resultant nanofibers can dramatically enhance the hydrogen-generation activity of ammonia borane under visible light irradiation. Such hydrogen-generation reaction can translate a molecular recognition event between folic acid and folate receptor to measurable pressure signal readout through a low-cost and portable pressure meter for target cancer cell detection. Limit of detections (LODs) down to 50 cells mL^{-1} in only 15 mins can be

achieved. This result is superior to those of the other reported methods, indicating the superiority of the new pressure-based sensor in terms of sensitivity. The present study establishes the pressure meter as a useful tool for early clinical point-of-care cancer diagnosis.

Graphic

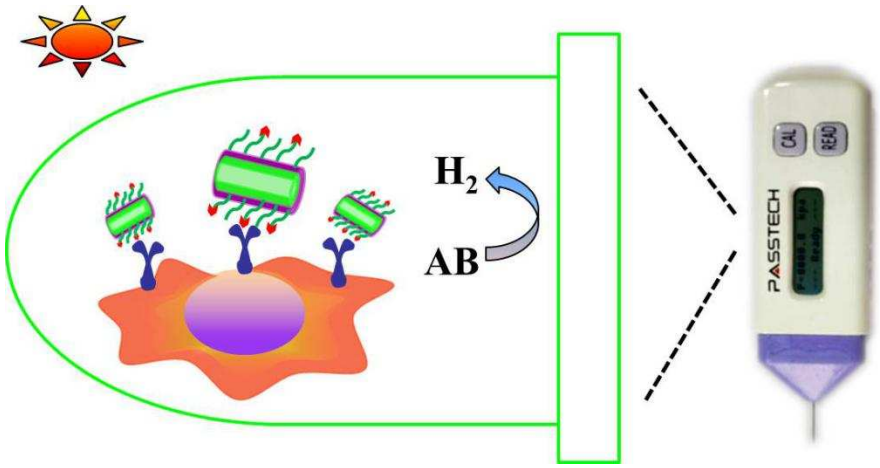

The development of portable sensors for rapid, on-site, and cost-effective detection of cancer cells is of vital significance to early diagnosis and timely prognosis of cancer.[1,2] Recently, optical,[3-7] electrochemical,[8-12] magnetic,[13,14] and mass spectrometric[15,16] assays for signal readout have been developed to detect the expression of cell surface receptors on cancer cells and generally regarded as the gold standards in laboratory scenarios. However, these assays have high cost, are affected by environmental interferences, and require bulk instrumentation and services of professional operators. Thus, their use in field work or specific point-of-care testing is restricted. Therefore, the development of portable sensors for rapid, on-site, and cost-effective detection of cancer cells is necessary.

In recent decades, alternative approaches based on totally different signaling principles using thermometer, barometer, and hygrometer readouts have been developed for simple and portable point-of-care testing.[17,18] For example, pressure-based bioassays, as signaling techniques, have

been successfully used to detect protein biomarker.[17] In such bioassays, the key step to highly sensitive detection is the conversion of a biomolecular recognition event into a highly-efficient gas-generation reaction. In addition, the reactant and product are nontoxic and environmentally friendly. Among all existing and emerging gas-generation reactions, ammonia borane (NH_3BH_3, denoted as AB) decomposition has attracted extensive concern because of the high hydrogen capacity of AB (19.6 wt.%). Notably, this process generates nontoxic H_2. Theoretically, the decomposition of 1 mmol of AB generates 67.2 mL of H_2 under standard conditions. If this solution is confined to a 1-mL tube, the pressure increases to over 6×10^6 Pa, which can be detected easily by a pressure meter. However, such a promising gas-generation reaction is rarely used for pressure-based bioassays. To date, many noble metals, such as Pd and Au,[19] exhibit highly efficient catalytic activity for AB dehydrogenation. However, their high cost, poor durability, and scarcity greatly restrict their use in large-scale commercial applications.

Semiconductor heterojunction photocatalysts have attracted significant attention[20] because they can achieve optimal solar light absorption and enhance surface reactivity. The catalytic activities of heterojunction nanomaterials are often superior to those of constituent elements because of their efficient exploitation of photo-generated electron/hole (e/h^+) pairs. This process accounts for the enhanced performance of heterojunction nanomaterials in relevant photoconversion processes. Among various oxide semiconducting materials, CuO[21] and Co_3O_4[22] photocatalysts have been the most well-known. Such oxide-based photocatalysts have been extensively studied as replacement for noble metal-based catalysts. We hypothesized that using such photocatalyst could significantly accelerate the reaction rate of AB dehydrogenation. This gas-generation photocatalyst can be linked with a molecular recognition event as a molecular recognition tool to construct a simple, rapid, sensitive, affordable, and specific cancer cell

detection method.

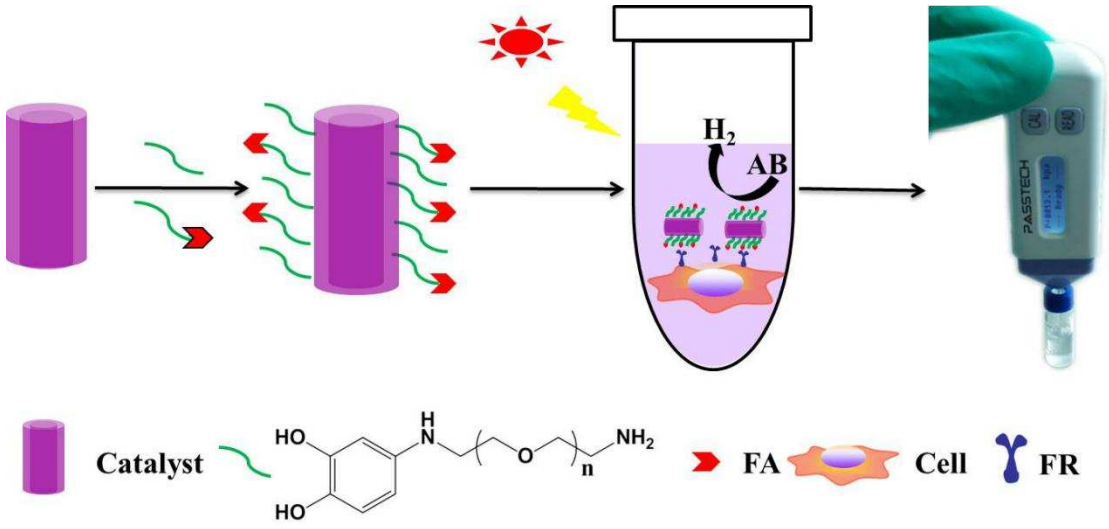

Scheme 1. Synthetic route of folic acid (FA)-conjugated tube-in-tube CuO/Co_3O_4 heterojunction nanofibers and its working principle for detection of cancer cells. The strong driving force elicited by specific interactions between overexpress folate receptor (FR) and FA caused the conjugation of functionalized CuO/Co_3O_4NFs onto the surface of the cancer cells. When added the ammonia borane (AB), hydrogen (H_2) can generate in the bottle, leading to a significant pressure increase in the reaction chamber allowing a sensitive readout by using a portable pressure meter.

In this study, we proposed a two-step and facile route to fabricate tube-in-tube CuO/Co_3O_4 heterojunction nanofibers (NFs) and demonstrated its usage in cancer detection based on pressure signal. The resulting heterojunction NFs exhibits excellent catalytic activity during AB hydrolysis for hydrogen generation. On the basis of these findings, we use catalyzed gas-generation reaction as signal readout for highly sensitive detection of cancer cells. The approach is based on the folate-conjugated CuO/Co_3O_4NFs, which provide dual functionality by binding to folate receptors, expressing cancer cells, and facilitating detection through the photocatalytic decomposition of the high hydrogen capacity of AB. This dual functionality results in significant pressure increase in the reaction chamber. The increase can be sensitively detected by a simple,

low cost, and portable pressure meter (scheme 1). To our best knowledge, this study is the first to use a pressure meter that detects the target cells simply and portably on the basis of AB decomposition.

EXPERIMENTAL SECTION

Materials. Polyacrylonitrile (PAN), polyvinylpyrrolidone (PVP), cupric acetate and cobalt (II) aetate tetrahydrate were all purchased from Macklin. Ammonia borane was purchased from HWRK CHEM. All the chemical agents were used as received without further purification. PEG-3,4-dihydroxy benzyl amine (DIB-PEG-NH_2) and PEG-3,4-dihydroxy benzyl amine -folic acid (DIB-PEG-NH-FA) were synthesised according to our previous work. [31]

Measurements. The morphology of the samples was investigated by field-emission scanning electron microscope (FE-SEM, FEI, Sirion 200). TEM measurements were carried out with a JEM-2100 (200 kV) instrument under ambient conditions through the deposition of ethanol dispersions of the nanomaterials on amorphous carbon-coated copper grids. X-ray powder diffraction patterns of the particles were recorded using a Bruker AXS D8 Advance diffractometer with $Cu_{K\alpha}$ radiation (l=1.5418 Å). X-ray photoelectron spectroscopy (XPS) measurements were performed using a PHI-5702 multifunctional spectrometer with $Al_{K\alpha}$ radiation. UV-Vis-NIR absorption spectra were carried out on a Agilent Cary 5000 UV-Vis-NIR Spectrophotometer. Photocatalysis was performed using Xenon lamp (HSX-F/UV 300), equipped with 400-800 nm filter. FT-IR characterization was carried out on a Bruker Vertex 70 FT-IR spectrometer.

Fluorescence microscopic images were viewed under a fluorescent microscope (Leica DR) equip ped with a digital camera (ORCA-ER, Hamamatsu). Cyclic voltammetry (CV) measurements were obtained by using CHI 760E electrochemical workstation. Glassy carbon and Pt electrodes

were used as working and counter electrodes, respectively. Ag/AgCl electrode worked as reference electrode. Cu and Co contents are determined by inductively coupled plasma-atomic emission spectrometry (ICP-AES, Varian VISTA-MPX).

The synthesis of CuO/Co_3O_4 heterojunction nanofibers. The preparation of CuO/Co_3O_4 1D nanostructures involves two steps. Briefly, a mixture of 1 g PVP, 1 g PAN, 1.5 mmol $Co(CH_3COO)_2.4H_2O$, 1.5 mmol $Cu(CH_3COO)_2 \cdot H_2O$ and 10 ml DMF was stirred at room temperature for 24 h, and then a viscous solution was obtained. Next, the precursor solution was loaded into a plastic syringe with a stainless steel nozzle ($8^{\#}$), which was connected to a high-voltage power supply. A high voltage of 18 kV was applied between the needle tip and aluminum foil collector with a distance of 17 cm and the spinning rate was controlled at 1 ml h^{-1}. Finally, the as-spun fibers were calcinated at 400 ℃ for 2 h at a heating rate of 4 ^{0}C min^{-1}. The other rate catalyst was synthesized by controlling the rate of salts added.

The synthesis of folic acid-functionalized CuO/Co_3O_4NFs. 0.02 g DIB-PEG-NH_2 and 0.002 g DIB-PEG-NH-FA[33] was added to 5 mL water solution containing 0.02 g CuO/Co_3O_4 NFs. After stirred for 12 h in the dark at room temperature, the mixtures were collected by centrifugation, washed with water, and then dispersed in water and dialyzed with H_2O for 24 h to remove unreacted organic molecules.

Catalytic Decomposition of Aminodiborane. To study the catalytic properties of the as-synthesized products, their catalytic activities were evaluated for the dehydrogenation of AB in aqueous solution under light or dark. In a typical experiment, 0.014 mmol catalyst and 3.3 mL water was added into a double walled glass tube with the neck connected to a gas burette through soft rubber tube. After stirring for 5 mins, 0.667 mmol of NH_3BH_3 was quickly added into the glass tube. The sealed reaction solution was stirred under light at 25 ± 1 ^{0}C (by using a

connected reflux water condenser). The volume of hydrogen gas generated from the hydrolysis reaction was measured using the water-displacement method. As a control, the same reaction was conducted in dark condition at room temperature. Recycling of CuO/Co_3O_4 NFs catalyst was tested under light at room temperature in water (3.3 mL) containing 0.028 mmol catalyst, with addition of AB (0.667 mmol) to the system in each cycle.

The apparent quantum efficiency (AQE) measurment. The apparent quantum efficiency (AQE) measurement: A 300-W Xe arc lamp was used as the light source for photocatalytic reaction. The measurement of AQE was performed using same amount reactions. We fixed the wavelength at 450 ± 10 nm for Vis irradiation. The laser power in the photocatalytic reaction was collected using a power meter (Newport; 843-R). The corresponding wavelengths captured for AQE calculation are located at 450 ± 10 nm. Thus, the AQE was calculated as the following equation, AQE =n/np × 100 %, in which n and np were denoted as the number of photos that generating product needed and the number of incident photons, respectively.

The apparent quantum efficiency (AQE) caculation. Under visible light irradiation (450 ± 10 nm) for CuO/Co_3O_4NFs within 1 min. The average intensity of irradiation was found to be 0.255 W and 0.072 W before and after the catalyst added to reaction flask by a power meter (Newport; 843-R). Total absorb light energy $\Delta E = (0.255 - 0.072) \times 1 \times 60 = 10.98$ J, n = 0.0344 mmol, energy per photon $E_0 = hc/\lambda = 6.63 \times 10^{-34} \times 3 \times 10^8/(450 \times 10^{-9}) = 4.42 \times 10^{-19}$ J, molor of photons $np = \Delta E/(E0 \times NA) = 10.98/(4.42 \times 10^{-19} \times 6.02 \times 10^{23}) = 0.0413$ mmol, AQE (initial) = n/np = 0.0344/0.0413 × 100 % = 83.3 %. With the same method, we can calculate the initial AQE for other catalysts, respectively.

Cyclic voltammetry (CV) analysis. To investigate the redox property of CuO, Co_3O_4 and CuO/ Co_3O_4, CV analysis was performed with a standard three-electrode system, which consists of an

Ag/AgCl reference electrode (0.01 M $AgNO_3$, 0.1 M TBAPF6 in CH_3CN), a platinum sheet working electrode and a platinum wire counter electrode. The electrolyte solution employed was 0.10 M TBAPF6 in freshly dried CH_3CN, and ferrocene/ferrocenium redox coupled (Fc/Fc+, -4.8 eV) was used as the reference material for all CV measurements. CV was recorded at 100 mV/s under a N_2 atmosphere.

Cytotoxicity assay and bioassay assay. In vitro cytotoxicity of the CuO/Co_3O_4NFs was evaluated by performing a methyl thiazolyl tetrazolium (MTT) assay of the HeLa cells incubated with the particles. Cells were seeded into a 96-well cell culture plate with a density of 5×10^3 cells per well in DMEM with 10% FBS at 37 °C under 5% CO_2 for 24 h. Then, the cells were incubated with the CuO/Co_3O_4NFs with different concentrations (0, 23, 34, 45, 56, 62 and 68 μg mL^{-1} in DMEM) for 24 h and 48 h at 37 °C under 5% CO_2. Thereafter, MTT (10 mL, 5 mg mL^{-1}) was added to each well and the plate was incubated for 4 h at 37 °C. After the addition of dimethyl sulfoxide (DMSO, 100 μL per well), the cell plate was allowed to stand at 37 °C for 15 mins. The optical density was measured at 492 nm using a microplate reader (Shanghai Sanco Instrument Co.,Ltd 318C-microplate reader).

HeLa cells, A549 cells, and NIH3T3 cells were maintained at 37 ºC, 5% CO_2 in a humidified incubator. Cells were plated in 6 well plate at density of 1×10^5 cells per well. After 24 h, cells were treated with different concentration of FA-CFO/Co_3O_4 NFs (23 to 68 μg mL^{-1}) for 1 h. Afterwards cells were washed with PBS buffer, the cells and 5mg AB were transferred to a 2ml tube and kept the liquid volume up to 1 mL. The pressure change in the tube was monitored by a portable home-made pressure meter under the visible light (LED lamp as the light source) for 15 mins. In another set of experiment, similar immunoassay were carried out using increasing number of HeLa cells (50 to 10^5 cells) keeping the concentration of FA-CuO/Co_3O_4 NFs constant

(23 μg mL^{-1}).

Detection of cancer cells in whole blood. HeLa cells were first spiked into healthy mouse or human blood to prepare artificial whole blood samples with concentrations of about 50, 10^2, 2×10^2, 3×10^2, 4×10^2, 5×10^2, 10^3, and 10^4 cells mL^{-1}. Then, 68 μg mL^{-1} of FA-CFO/Co_3O_4 NFs was added into the above blood samples and incubated for 1h. Afterwards blood samples were washed with PBS buffer, the blood samples and 5mg AB were transferred to a 2 ml tube and kept the liquid volume up to 1 mL. The pressure change in the tube was monitored by a portable home-made pressure meter under the visible light (LED lamp as the light source) for 15 mins. In order to identify that HeLa cells existed in whole blood sample, the three-color immunocytochemistry method was used. First, HeLa cells and blood cells were sequentially treated with 4% paraformaldehyde in PBS for 20 mins and 20 μL of methanol for 10 mins. Then, the cells were sequentially stained with 50 μL of anti-CD45 stock solution (50 μL of antibody stock solution in 1 mL of PBS) for 45 mins, 50 μL of anti-CK stock solution (50 μL of antibody stock solution in 1 mL of PBS) for 45 mins, and 20 μL of Hoechst solution (2 μg mL^{-1} Hoechst in PBS) for 15 mins, respectively. Finally, cells were imaged by using Leica DR microscope.

RESULTS AND DISCUSSION

Synthesis and Characterization of the Catalyst. CuO/Co_3O_4NFs were synthesized using a certain amount of $Co(CH_3COO)_2$/$Cu(CH_3COO)_2$, polyvinylpyrrolidone (PVP), and polyacrylonitrile (PAN) by a simple method involving two steps, namely, electrospinning and thermal treatment. As shown in Figure 1, the formed CuO/Co_3O_4NFs perfectly maintained the 1D nanostructure. In addition, compared with PAN@PVP/$Co(CH_3COO)_2$/$Cu(CH_3COO)_2$ composite NFs, the formed CuO/Co_3O_4NFs had a rough surface with many nanoparticles (NPs), which formed a unique tubular structure. The formed CuO/Co_3O_4NFs were further confirmed by

the transmission electron microscope (TEM) images (Figure 1C and D). The CuO/Co_3O_4NFs were composed of NPs, and each nanoparticle was attached to several other NPs. Many nanopores were observed to be within the spaces between the adjacent NPs. Apparently, the dual tubular structure of the CuO/Co_3O_4 NFs possessed well-separated walls along nearly their entire length, and the average diameter of the outer tubes and inner tube was approximately 210 and 100 nm, respectively (Figure 1C). Meanwhile, the high-resolution HRTEM images of the CuO/Co_3O_4NFs are shown in Figure 1D. The simultaneous presence of crystalline Co_3O_4 and CuO crystal lattices were observed in the CuO/Co_3O_4NFs. An intimate contact between CuO and Co_3O_4 was also observed. Figure 1D shows that an interplanar distance of 0.47 nm can be indexed as the interplanar distance of the Co_3O_4 (111) planes.[23] The interplanar distances of 0.235 nm agreed well with the lattice spacing of the (111) planes of the hexagonal wurtzite CuO.[24] These results confirmed that heterostructures were formed between Co_3O_4 and CuO NPs in the CuO/Co_3O_4NFs. The local composition of the resulting CuO/Co_3O_4NFs was also examined through high angle annular darkfield scanning transmission electron microscopy (HAADFSTEM), corresponding elemental mapping (Figure 1E–H), and energy-dispersive X-ray spectroscopy (EDX; Figure S1). The results clearly showed the presence of Cu, Co, and O elements.

Figure 2A shows the XRD patterns of the as-synthesized nanofibers. The CuO/Co_3O_4 NFs had two sets of diffraction peaks, which were correspondingly ascribed to the cubic spinel Co_3O_4 (JCPDS card no. 01-076-1802) and CuO phase (JCPDS-ICDD 05-0661). No characteristic peaks for impurity, such as $CuCo_2O_4$, were observed, suggesting that Co_3O_4 and CuO formed heterojunction in the nanofibers. Moreover, typical X-ray photoelectron spectroscopy (XPS) spectra (Figure S2) showed the presence of Co, Cu, O, and adventitious C in the CuO/Co_3O_4

nanofibers. As observed in Figure S2b, two peaks at binding energies of 933.9 and 953.9 eV in Cu 2p XPS spectra could be assigned to Cu 2p3/2 and Cu 2p1/2, respectively. The peaks shift 0.3 eV compared to CuO. [25] The above values indicate a normal state of Cu^{2+} in the CuO/Co_3O_4 nanofibers. As for Co peaks, the binding energies located at ~780.4 and ~795.5 eV can be assigned to Co 2p3/2 and Co 2p1/2 (Figure S2c), together with a spin-energy separation of around 15 eV, demonstrating the presence of a Co_3O_4 phase. [26] Nitrogen adsorption measurement results (Figure 2B) revealed that the CuO/Co_3O_4NFs exhibited type IV isotherm behavior with H3 hysteresis, implying that the obtained fibers were mesoporous. The distribution of Barrett-Joyner-Halenda pore sizes determined from the adsorption branches peaked at ~25 nm.

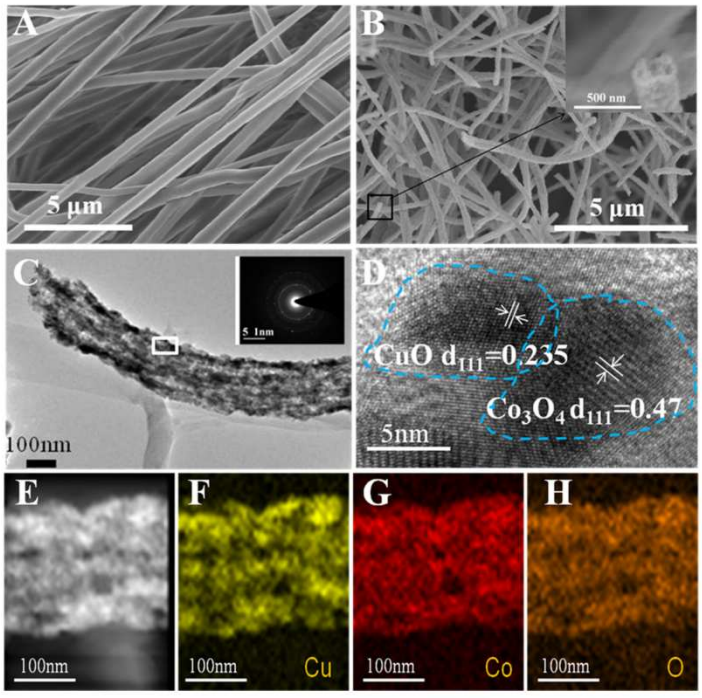

Figure 1. SEM images of precursor NFs (A) and CuO/Co_3O_4 NFs (B); C) TEM image and SAED pattern of CuO/Co_3O_4 NFs; D) HRTEM images of CuO/Co_3O_4 NFs; E) The corresponding STEM-EDS elemental mapping images of Cu (F), Co (G), and O (H) in CuO/Co_3O_4 nanofibers.

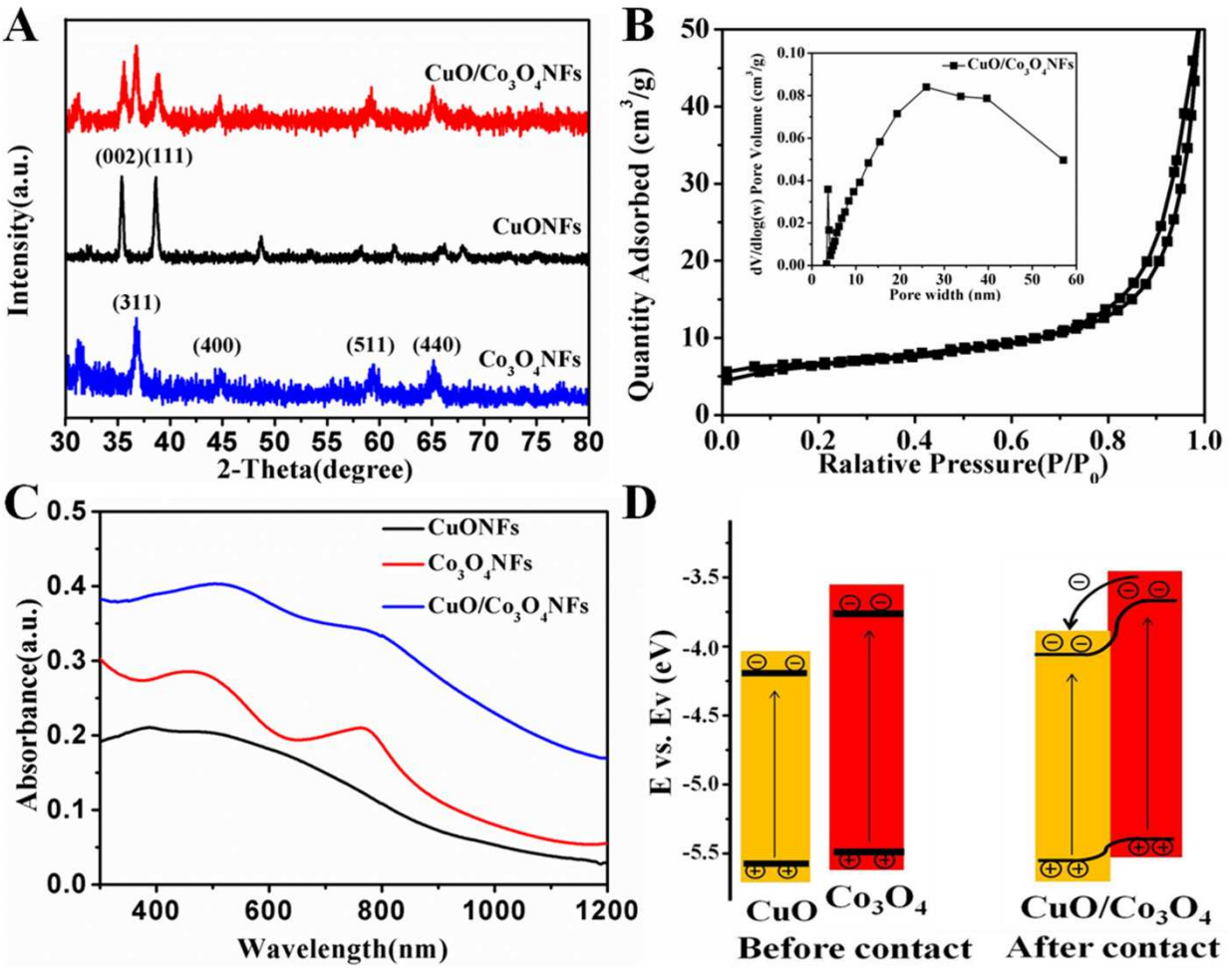

Figure 2. A) XRD patterns of CuONFs, Co_3O_4NFs, and CuO/Co_3O_4NFs; B) N_2 adsorption/desorption isothermals of CuO/Co_3O_4 NFs; C) UV-vis spectra of CuONFs, Co_3O_4NFs, and CuO/Co_3O_4NFs; D) Band diagram and mechanism of charge separation for p-Co_3O_4/p-CuO heterojunction.

Figure 2C shows the UV-vis spectra of the CuONFs, Co_3O_4NFs, and CuO/Co_3O_4NFs. The absorption edges of the CuONFs appeared at 832 nm and corresponded to the band gap energies of 1.49 eV. The Co_3O_4NFs exhibited two main absorption bands, and the absorption edges appeared at 663 nm and corresponded to the band gap energies of 1.87 eV. These values were close to the reported values of CuO (1.40 eV) and Co_3O_4 (1.89 eV).[27] The CuO/Co_3O_4NFs indicated that two evident absorption bands were present, and these bands were ascribed to the characteristic absorption of CuO and Co_3O_4. We estimated the conduction bands, valence band

edges, and Eg values of CuO and Co_3O_4 (Figure 2D) according to the cyclic voltammetry (Figure S4) test and Tauc plots (Figure S3). Since the value of E_{CB} for Co_3O_4 is more negative than that of CuO, under visible light illumination, the excited electrons of Co_3O_4 can be transported to the conduction band of CuO. While the photogenerated holes on the valence of Co_3O_4 cannot transfer to that of CuO, so the combination of electrons and holes can be prevented.[28] As a consequence, the separation of photogenerated electron-hole pairs is significantly improved. Thus, we proposed a mechanism of charge separation for CuO/Co_3O_4 heterojunction (Figure 2D).

Catalytic Properties and Mechanism. The prepared CuO/Co_3O_4NFs were first tested for the catalytic hydrolysis of AB to generate H_2 under dark and visible light irradiation ($\lambda > 420$ nm) at room temperature. The activities of the catalysts under light were enhanced to a greater extent compared with those under dark environment (Figure 3A). Under light, the reaction can be completed within 4.5 mins, which is faster than the time undertaken by the same reaction under dark environments (8 mins). The contribution of the thermal effects induced by visible-light irradiation was eliminated at the same reaction temperature (25 ± 1 °C) for AB hydrolysis (by using a connected reflux water condenser) under dark conditions and visible-light irradiation. Under visible light irradiation, the photocatalytic property of the CuO/Co_3O_4NFs toward AB hydrolysis was tested and compared with those of CuONFs, Co_3O_4NFs, and physical mixture of CuO NFs and Co_3O_4 NFs at 25 ± 1 °C. Figure 3B shows the amount of H_2 generated as a function of reaction time. Evidently, the H_2 generation rates of the CuO/Co_3O_4 catalyst were enhanced to a greater extent compared with those of their monometallic or mixture counterparts. Simultaneously, a quantum efficiency of 83.3% at 450 ± 10 nm was achieved by the CuO/Co_3O_4NFs. This efficiency was the highest among the efficiencies of all as-prepared nanofibers (Figure S6). The highest photoactivity can be ascribed to the formation of the

nanojunction between the CuO and Co_3O_4, and the generated electrons enriched on the conduction band of Co_3O_4 enhanced the photocatalytic activity of the CuO/Co_3O_4 catalyst for the AB dehydrogenation (Figures S7 and 8). In addition, the resulting CuO/Co_3O_4 catalyst had high cycle stability (Figures S9, 10, and 11).

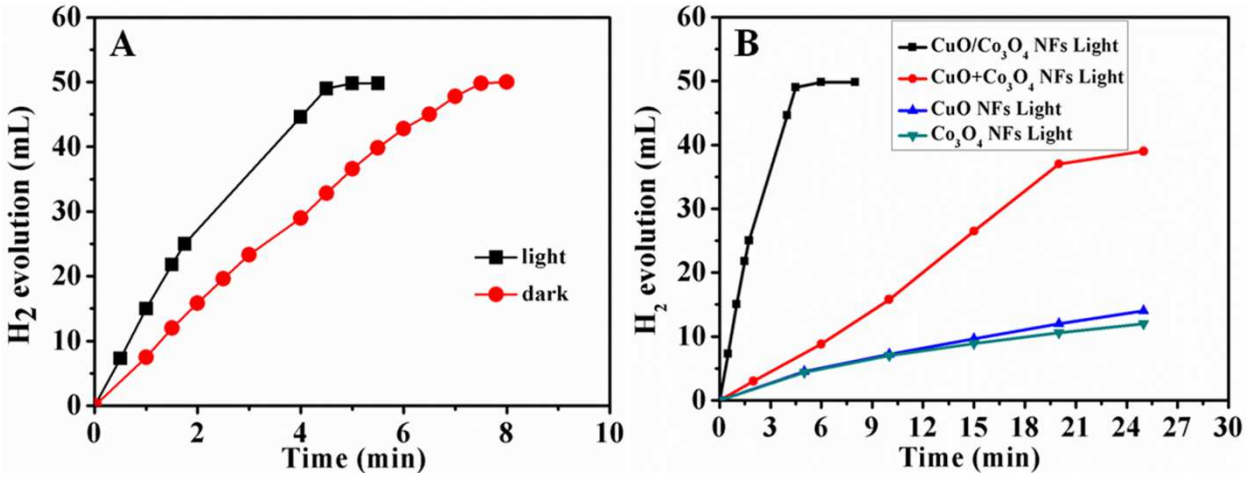

Figure 3. A) Hydrogen evolution in aqueous solution(3.3 mL) containing fixed amount of AB (0.65 mmol) and CuO/Co_3O_4NFs(0.014 mmol) under or without light at 298 K; B) Relationship between dehydrogenation rate of AB (0.65 mmol) and different catalysts (0.014 mmol) at 298 K in water(3.3 mL) under light.

Cytotoxicity assay and bioassay assay. Given the high photocatalytic activity towards AB hydrolysis, CuO/Co_3O_4NFs was designed as a sensing platform for highly sensitive detection of cancer, which was based on pressure response. In order to improve the dispersity of CuO/Co_3O_4NFs in water and enhance the targeting ability of the CuO/Co_3O_4NFs for cancer cells, we used the PEG-3, 4-dihydroxy benzyl amine (DIB-PEG-NH_2) and PEG-3, 4-dihydroxy benzyl amine-folic acid (DIB-PEG-NH-FA) to modify the CuO/Co_3O_4NFs (Scheme 1). The detailed characteristics were provided in the supporting information (Figures S12 and 13). Folic acid is a high-affinity ligand for the folate receptor (FR), and has been widely used for targeted delivery of FA-conjugated molecular probes or nanoparticles to FR-overexpressing cancer cell lines (e.g.,

HeLa and KB cell lines).[29,30] Cytotoxic activity was evaluated before the application of CuO/Co_3O_4NFs for cancer cell detection. As shown in Figure S14, the cell viability of CuO/Co_3O_4NFs for HeLa cells remained more than 75% upon incubation with CuO/Co_3O_4NFs at 68 μg mL^{-1} concentration for 48 h, indicating the low cytotoxicity of the CuO/Co_3O_4NFs. HeLa cells and A549 cells that overexpress folate receptor were used to test the performance of the selectivity of FA-CuO/Co_3O_4NFs.[29] In the control experiments, we used NIH3T3 cells that do not express folate receptors.[31] Three kinds of cells were incubated with FA-CuO/Co_3O_4NFs for 1 h. The cells were then washed with 1× PBS, and incubated with AB (5 mg). The pressure change in the tube was monitored under visible light by a portable home-made pressure meter. As shown in Figure 4A, HeLa and A549 cells with the same cell number (6×10^5) exhibited significant pressure change, whereas the NIH3T3 cells provided only negligible signals. This result clearly indicated that the discrimination between FA-positive cancerous cells and normal cells can be easily recognized through pressure changes.

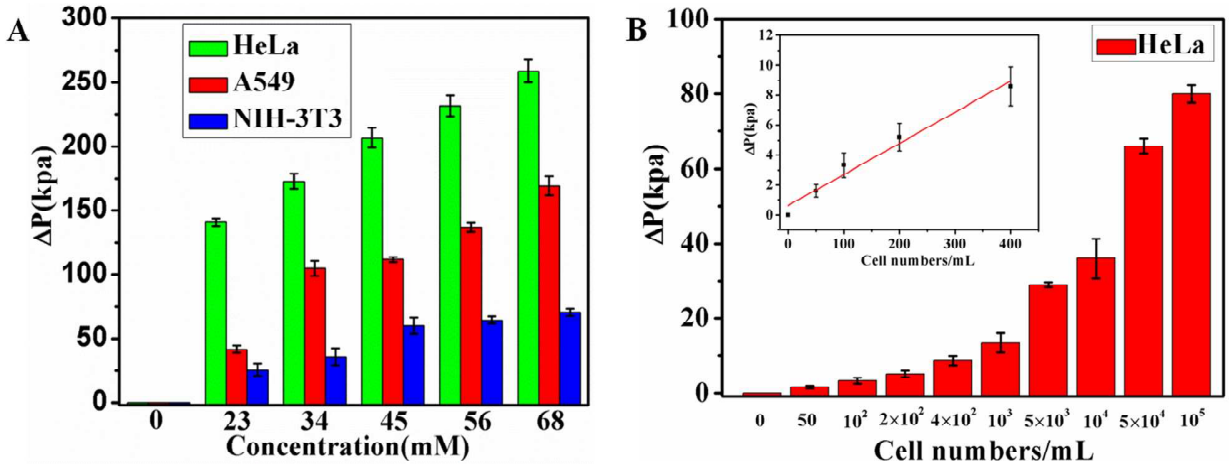

Figure 4. Pressure determination of the expression of the folate receptor in cancer cells using FA-CuO/Co_3O_4NFs. A) Pressure-change profiles of cells after incubation with FA-CuO/Co_3O_4NFs for 1 h and then addition of AB. B) quantitatively detect HeLa cells using FA-

CuO/Co_3O_4 NFs and AB based on pressure-change. Values are expressed as mean ±SD.

We then investigated the limit of detection (LOD) and detection dynamics of the biosensor assay. HeLa cells at varying concentrations were incubated with FA-CuO/Co_3O_4 NFs. As shown in Figure 4B, with the increase of cells number, the measured ΔP continuously increased. Moreover, the ΔP against cells number showed a good linear correlation, realizing an LOD of 50 cells mL^{-1}. The LOD obtained was lower than those obtained by other reports,[32] which demonstrating the excellent sensitivity of FA-CuO/Co_3O_4NFs for quantitative bioanalysis. The detection dynamic curve displayed in Figure S15 indicated that the gas pressure increases over incubation time. However, the incubation time of 15 mins was basically sufficient to discriminate the interactions between the FA-CuO/Co_3O_4NFs and HeLa cells. Therefore, such pressure change detection platform is well suited for highly sensitive and rapid cancer detection in clinical and point-of-care settings.

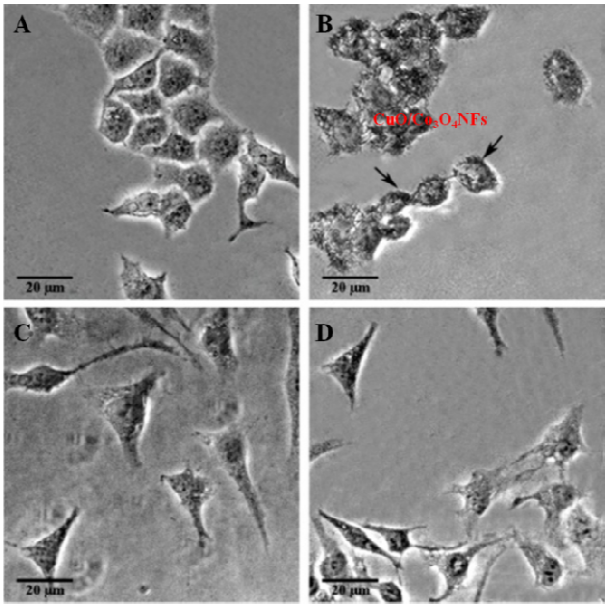

Figure 5. Confocal images of HeLa cells alone (A), HeLa cells incubated with CuO/Co_3O_4 for 1 h (B), NIH3T3 cells alone (C), and NIH3T3 cells incubated with CuO/Co_3O_4 for 1 h (D).

We also analyzed the deposition of CuO/Co_3O_4NFs on the cell surface. Confocal images were used to determine whether CuO/Co_3O_4NFs are present on the cell surface. Figure 5A, 5B, and S16 shows that the strong driving force elicited by specific interactions between overexpress folate receptor and FA caused the conjugation of functionalized CuO/Co_3O_4NFs onto the surface of the HeLa cells in the presence of the target cells. Moreover, no nanofiber precipitate was detected on the surface of the negative control cells (Figure 5 C and D).

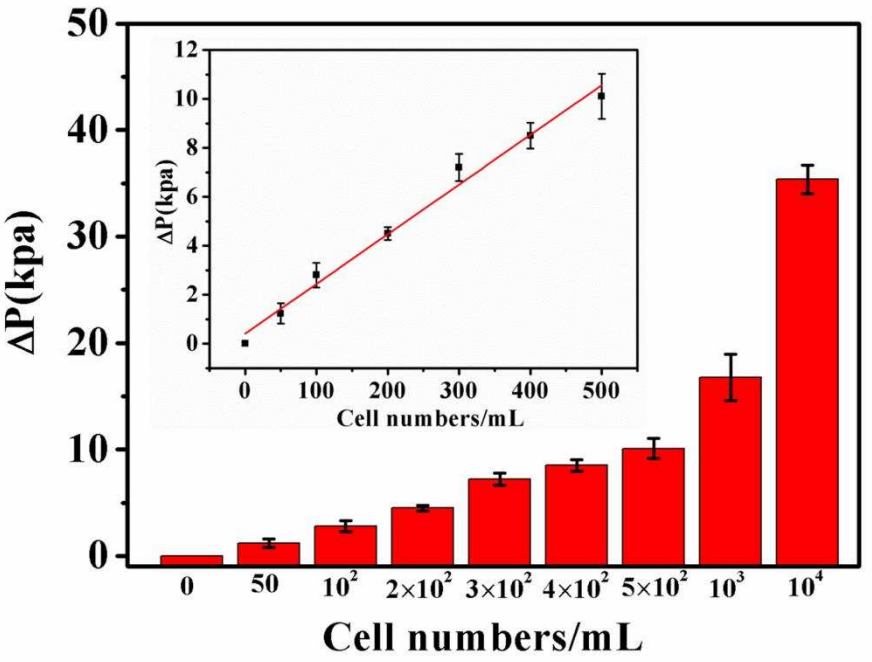

Figure 6. Detection performance of FA-CuO/Co_3O_4NFs for artificial whole blood samples spiked with HeLa cells. The capture efficiency of prestained HeLa cells is achieved on anti-EpCAM-coated HTiNS coatings for artificial whole blood samples with concentration of 50, 10^2, 2×10^2, 3×10^2, 4×10^2, 5×10^2, 10^3, and 10^4 cells mL^{-1}. Values are expressed as mean ±SD.

To demonstrate the potential clinical application, the sensor was also used to detect HeLa in artificial whole blood. Briefly, we prepared the artificial whole blood samples by spiking healthy mouse blood with HeLa cells at concentrations of approximately 50, 10^2, 2×10^2, 3×10^2, 4×10^2, 5×10^2, 10^3, and 10^4 cells mL^{-1}. As shown in Figure 6, the measured ΔP also increased linearly

with the cells number, an LOD of 50 cells mL^{-1} was obtained. Such a sensitive detection method was confirmed in human blood samples by spiking healthy human blood with HeLa cells (Figure S16). When the CuO/Co_3O_4 NFs kept in blood and stayed for 24 hours, we checked the stability of CuO/Co_3O_4 NFs by using the XRD and SEM. As shown in Figure S17, there is not change of composition and morphology. Therefore, the reagent is stability in detection system. In addition, we employed the three-color immunocytochemistry method based on PE-labeled anti-CK (CK, a protein marker for epithelial cells), FITC-labeled anti-CD45 (CD45, a marker for white blood cells), and Hoechst for nuclear staining to confirm the HeLa cells in a artificial whole blood sample. As shown in Figure 7, HeLa cells can be clearly identified from whole blood sample. Therefore, these results show the potential biomedical application of hydrogen-generation CuO/Co_3O_4 heterojunction nanofibers based on pressure-based bioassays for early diagnosis and monitoring of cancer patients.

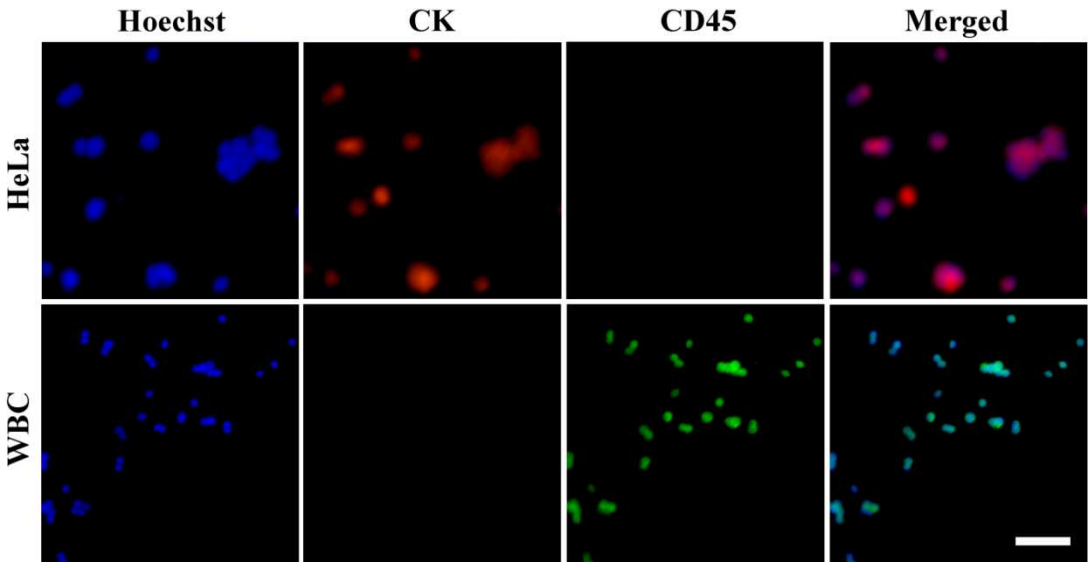

Figure 7. Three-color immunocytochemistry method for identifying HeLa cells from white blood cells (WBCs) including Alexa Fluor488-labeled anti-CK (CK, a protein marker for epithelial cells), FITC-labeled anti-CD45 (CD45, a marker for WBCs) and Hoechst for nuclear staining. (Scale bar = 20 μm).

CONCLUSION

In summary, for the first time, we have designed a simple and general method based on gas-generation CuO/Co_3O_4 heterojunction nanofibers and a portable pressure meter for inexpensive, rapid, portable, user-friendly, and quantitative detection of specific cancer cells. This method provided an excellent dynamic range of 50 to 10^5 cells mL^{-1} for Hela cells with a detection limit of at least 50 cells mL^{-1} in only 15 mins. In addition, such pressure-based bioassays can efficiently detect Hela cells from artificial whole blood samples with high sensitivity. The excellent performance of the method is attributed to the highly efficient photocatalytic activity of CuO/Co_3O_4 NFs during AB dehydrogenation and high hydrogen capacity of AB. To the best of our knowledge, this is the most sensitive detection method for cancer cells. The approach proposed in this study has the potential to perform early clinical point-of-care cancer diagnosis. It can be used in the field and by the public at home because of its simple design and operation, low cost, portability, and excellent sensitivity and its ability to recognize different cancer cells.

ASSOCIATED CONTENT

Supporting Information

Characterizations, Supporting Figures and Tables are available free of charge via the Internet at http://pubs.acs.org.

AUTHOR INFORMATION

Corresponding Author

*E-mail: wangbd@lzu.edu.cn; luxq@tju.edu.cn.

ACKNOWLEDGMENTS

The work was supported by the National Natural Science Foundation of China (21671088, 21401091, 21431002 and 21501080, 21575115 and 21327005), and Fundamental Research Funds for the Central Universities (lzujbky-2017-105).

REFERENCES

(1) R. Kumar, J. Han, H. Lim, W. Ren, J. Lim, J. Kim, J. Kim. *J. Am. Chem. Soc.* **2014**, 136, 17836−17843.

(2) M. Ebert, M. Korc, P. Malfertheiner, C. Rocken. *Proteome Res.* **2006**, 5, 19−25.

(3) H. Liu, S. Xu, Z. He, A. Deng, J. Zhu. *Anal. Chem.* **2013**, 85, 3385−3392.

(4) M. Judit, G. Patricia, M. Matteo, G. Eduardo, A. Ramon, G. Luca. *Angew. Chem. Int. Ed.* **2017**, 56, 2381 –2385.

(5) X. Zheng, H. Tang, C. Xie, J. Zhang, W. Wu, X. Jiang. *Angew. Chem. Int. Ed.* **2015**, 54, 8094 –8099.

(6) X. Wu, M. Wu, J. Zhao. *Nanomed. Nanotechnol.* **2014**, 10, 297−312.

(7) Z. F. Chang, L. M. Jing, B. Chen, M. S. Zhang, X. L Cai, J. J. Liu, Y. C. Ye, X. D. Lou, Z. J. Zhao, B. Liu, J. L. Wang and B. Z. Tang, *Chem. Sci.*, **2016**,7, 4527-4536.

(8) J. Zhao, L. Zhu, C. Guo, T. Gao, X. Zhu, G. Li. *Biosens. Bioelectron.* **2013**, 49, 329−333.

(9) P. Chandra, H. Noh, Y. Shim. *Chem. Commun.* **2013**, 49,1900−1902.

(10) Y. Zhu, P. Chandra, Y. Shim. *Anal. Chem.* **2013**, 85, 1058−1064.

(11) M. Yan, G. Sun, F. Liu, J. Lu, J. Yu, X. Song. *Anal. Chim. Acta.* **2013**, 798, 33−39.

(12) T. Li, Q. Fan, T. Liu, X. Zhu, J. Zhao, G. Li. *Biosens. Bioelectron.* **2010**, 25, 2686−2689; L. Wang, A. Ambrosi, M. Pumer, *Anal. Chem.*, **2013**, 85, 6195-6197.

(13) S. Bamrungsap, T. Chen, M. Shukoor, Z. Chen, K. Sefah, Y. Chen, W. Tan. *ACS Nano*. **2012**, 6, 3974−3981.

(14) J. S. Basuki, L. Esser, H. T. T. Duong, Q. Zhang, P. Wilson, M. R. Whittaker, D. M. Haddleton, C. Boyer and T. P. Davis, *Chem. Sci*., **2014**, 5, 715-726.

(15) G. Liu, Eggler, B. Dietz, A. Mesecar, J. Bolton, J. Pezzuto, R. Breemen, *Anal. Chem*. **2005**, 77, 6407-6414.15

(16) J. Wang, T. Christison, K. Misuno, L. Lopez, A. Huhmer, Y. Huang, S. Hu. *Anal. Chem.* **2014**, *86*, 5116–5124.

(17) Z. Zhu, Z. Guan, D. Liu, S. Jia, J. Li, Z. Lei, S. Lin, T. Ji, Z. Tian, C. Yang. *Angew. Chem. Int. Ed.* **2015**, 54, 10448 –10453; b) H. Xie, Y. Li, Y. Lei, Y. Liu, M. Xiao, C. Gao, D. Pang, W. Huang, Z. Zhang, G. Zhang, *Anal.Chem.*,**2016**, 88, 11115-11122.

(18) Y. Xiang, Y. Lu. *Nat Chem.* **2011**, 3, 697–703.

(19) a) O. Metin, S. Duman, M. Dinç, S. Özkar, *J. Phys. Chem. C.* **2011**, 115, 10736-10743; b) L.-T. Guo, Y.-Y. Cai, J.-M. Ge, Y.-N. Zhang, L.-H. Gong, X.-H. Li, K.-X. Wang, Q.-Z. Ren, J. Su, J.-S. Chen, *ACS Catal*. **2015**, 5, 388-392.

(20) a) J. Li, S. K. Cushing, P. Zheng, T. Senty, F. Meng, A. D. Bristow, A. Manivannan, N. Wu, *J. Am. Chem. Soc*. **2014**, 136, 8438-8449; b) M. McEntee, A. Stevanovic, W. Tang, M. Neurock, J. T. Yates, Jr., *J. Am. Chem. Soc*. **2015**, 137, 1972-1982; c) P. Li, Z. Wei, T. Wu, Q. Peng, Y. Li, *J. Am. Chem. Soc*. **2011**, 133, 5660-5663.

(21) a) F. M. Auxilia, S. Ishihara, S. Mandal, T. Tanabe, G. Saravanan, G. V. Ramesh, N. Umezawa, T. Hara, Y. Xu, S. Hishita, Y. Yamauchi, A. Dakshanamoorthy, J. P. Hill, K. Ariga, H. Abe, *Adv. Mater.* **2014**, 26, 4481-4485; b) C. Hou, M. Zhang, T. Kasama, C. Engelbrekt, L. Zhang, H. Wang, Q. Chi, *Adv. Mater.* **2016**, 28, 4097-4104; c) u. In, D. Vaughn , R. Schaak. *Angew. Chem. Int. Ed.* **2012**, 51, 3915 –3918.

(22) a) L. R. Baker, C. M. Jiang, S. T. Kelly, J. M. Lucas, J. Vura-Weis, M. K. Gilles, A. P. Alivisatos, S. R. Leone, *Nano Lett.* **2014**, 14, 5883-5890; b) Q. Shen, Z. Chen, X. Huang, M. Liu, G. Zhao, *Environ. Sci. Technol.* **2015**, 49, 5828-5835; c) Y. Shen, B. Luo, J. Zhang, *Anal. Chem.*, **2016**, 88, 1617-1624.

(23) C. Ma, Z. Mu, J. Li, Y. Jin, J. Cheng, G. Lu, Z. Hao, S. Qiao, *J. Am. Chem. Soc*. **2010**, 132, 2608-2613.

(24) Y. Duan, X. Liu, L. Han, S. Asahina, D. Xu, Y. Cao, Y. Yao, S. Che, *J. Am. Chem. Soc*. **2014**, 136, 7193-7196.

(25）D. Gao, G. Yang, J. Li, J. Zhang, J. Zhang, D. Xue, *J. Phys. Chem. C*, **2010**, 114, 18347-18351.

(26）G. Armatas, A. Katsoulidis, D. Petrakis, P. Pomonis, M. Kanatzidis, *Chem. Mater.*, **2010**, 22, 5739-5746.

(27) a) Y. Ge, Z. H. Shah, C. Wang, J. Wang, W. Mao, S. Zhang, R. Lu, *ACS Appl. Mater. Interfaces* . **2015**, 7, 26437-26444; b) X. Chang, T. Wang, P. Zhang, J. Zhang, A. Li, J. Gong, *J. Am. Chem. Soc*. **2015**, 137, 8356-8359.

(28) M. Long, W. Cai, J. Cai, B. Zhou, X.e Chai, Y. Wu, *J. Phys. Chem. B.* **2006,** 110, 20211-20216.

(29) A. Asati, S. Santra, C. Kaittanis, S. Nath, J. M. Perez, *Angew. Chem. Int. Ed*. **2009**, 48, 2308-2312.

(30) M. E. Nelson, N. A. Loktionova, A. E. Pegg, R. C. Moschel, *J. Med. Chem*. **2004**, 47, 3887.

(31) F. Bottero, A. Tomassetti, S. Canevari, S. Miotti, S. Menard and M. I. Colnaghi, *Cancer Res*. **1993**, 53, 5791–5796.

(32) Y. Li, Y. Zhang, M. Zhao, Q. Zhou, L. Wang, H. Wang, X. Wang, L. Zhan, *Chem. Commun.* **2016**, 52, 3959-3961.

(33) Y. Peng, Z. Wang, W. Liu, H. Zhang, W. Zuo, H. Tang, F. Chen, B. Wang, *Dalton Trans.* **2015**, 44, 12871–12877.